Inkjet-printed microgel-based etalon sensor

Kontaxi, G.; Lugtmeijer, T. J.; Serpe, M. J.; Bazyar, H.

DOI
10.1063/5.0252901

Publication date
2025

Document Version
Final published version

Published in
Biomicrofluidics

RESEARCH ARTICLE | AUGUST 19 2025

Inkjet-printed microgel-based etalon sensor

G. Kontaxi ; T. J. Lugtmeijer ; M. J. Serpe ; H. Bazyar

Biomicrofluidics 19, 044101 (2025)
https://doi.org/10.1063/5.0252901

Biomicrofluidics ARTICLE pubs.aip.org/aip/bmf

Inkjet-printed microgel-based etalon sensor

Cite as: Biomicrofluidics 19, 044101 (2025); doi: 10.1063/5.0252901
Submitted: 12 December 2024 · Accepted: 17 July 2025 ·
Published Online: 19 August 2025

G. Kontaxi,[1] T. J. Lugtmeijer,[2] M. J. Serpe,[3] and H. Bazyar[1,a)]

AFFILIATIONS

[1]Transport Phenomena, Department of Chemical Engineering, Faculty of Applied Sciences, Delft University of Technology, Van der Maasweg 9, 2629HZ Delft, The Netherlands
[2]Engineering Thermodynamics, Process & Energy Department, Faculty of Mechanical Engineering, Delft University of Technology, Leeghwaterstraat 39, 2628CB Delft, The Netherlands
[3]Department of Chemistry, University of Alberta, Edmonton T6G 2G2, Canada

[a)]**Author to whom correspondence should be addressed:** h.bazyar@tudelft.nl

ABSTRACT

Stimuli-responsive microgel-based etalons are promising optical and bio-sensors. These sensors play a pivotal role in modern healthcare by enabling rapid biomolecule detection, contributing to organ-on-chip applications and early disease diagnosis. This study investigates the suitability of poly(N-isopropylacrylamide) (pNIPAm)-based microgels for inkjet printing, focusing on optimizing their properties for effective deposition. Key parameters, including surface tension, viscosity, and particle size, are characterized to ensure compatibility with inkjet-printing requirements. The addition of surfactants tunes the suspensions' properties to be in line with the requirements of inkjet printing. Jetting of pNIPAm-based microgels on gold-coated substrates forms a cohesive drop in a range of a few millimeters. Optical and scanning electron microscopy confirm the formation of a uniform microgel layer. The optical reflectance spectroscopy results indicate that inkjet-printed microgel-based etalons can effectively respond to changes in temperature and glucose concentration. In-liquid atomic force microscopy demonstrates the swelling dynamics of the microgels in different glucose concentrations, shedding light on their response dynamics. Our work demonstrates, for the first time, the feasibility of printing microgels in a controlled way, fabricating biocompatible inkjet-printed microgel-based etalon sensors with precise dimensions. The size precision and the sensitive monitoring capabilities of biomolecules hold great promise for *in situ* and continuous sensing in a wide range of biological and organ-on-chip applications.

I. INTRODUCTION

Real-time biomolecule sensing enables the rapid detection of target analytes and the conversion of these interactions into interpretable signals, forming the foundation of advanced biosensing technologies.[1] Biosensors play a crucial role in modern healthcare by enabling rapid and sensitive detection of biomolecules, facilitating early disease diagnosis and opening the door for personalized medicine, also offering a significant contribution to organ-on-chip applications.[2–4] With the growing demand for precision and sensitivity in user-friendly platforms that combine high accuracy with scalability and versatility,[5] the ability to achieve controlled deposition of sensing materials is paramount for ensuring consistent performance and reproducibility across applications.

Advances in materials science and engineering have led to new perspectives in the field of chemical and biochemical sensors with stimuli-responsive polymers having attracted great scientific interest.[6] Their ability to change their physical and/or chemical properties in response to stimuli, such as temperature, pH, light, or the presence of an analyte,[7–9] has rendered them as key materials in many fields including drug-delivery,[10] cancer therapy,[11] and sensing.[12] For diagnostics, the development of microgel-based etalon sensors provides an optical response to a variety of stimuli such as temperature, pH, and various biomolecules.[12–14]

Microgel-based etalon sensors use the Fabry–Pérot etalon construct, where changes in the distance between the two mirror layers, separated by a dielectric layer, lead to reflection/transmission of different wavelengths of light.[15,16] The maximum wavelength of a reflectance peak, λ, can be estimated using (1),

$$\lambda = \frac{2nd\cos(\theta)}{m} \tag{1}$$

and depends on the refractive index of the dielectric layer, n; the mirror–mirror distance, d (nm); the angle of incident light relative to the normal, θ (°); and the order of the reflected peak, m (an integer).[15]

The microgel-based etalons typically consist of a thin Au layer of 15 nm deposited on a glass substrate, followed by deposition of thermo-responsive poly(*N*-isopropylacrylamide) (pNIPAm)-based microgels as a monolithic layer. A second thin Au layer (15 nm) is then deposited on the microgel layer[12] (Fig. 1). In this, microgel-based etalon structure microgels are used to form the dielectric layer, and their swelling or de-swelling response to the stimuli alters the distance of the two Au layers, leading to a change in λ. This change can be monitored using optical reflectance spectroscopy. The changes in the wavelength of reflected light are mainly depending on the distance of the Au layers and, thus, on the thickness and the uniformity of the microgel layer.[5]

The deposition of the microgels on the Au-coated substrate plays a key role in the optical properties of the etalons. The main studied protocol for microgels deposition is the "paint-on" protocol.[17] Using this protocol, a uniform solution of microgels is spread on the Au-coated substrate, and the sample is left to dry for 2 h prior to the removal of the excess microgels by rinsing it with de-ionized (DI) water. While this method is simple, reproducibility poses a challenge since it is a manual technique and even if a standard volume of aliquot is used, the spreading may vary among different samples. Another concern is the minimum area of coating as spreading evenly an area of $3 \times 3\,\text{mm}^2$ or smaller might be quite a challenge without offering adequate results. Another method that has been used for the microgel film deposition is spin-coating.[18] Spin-coating of microgel's aliquot at 3000 rpm for 30 s on the Au-coated substrate forms a uniform, monolithic microgel film. The samples are dried for 2 h, and rinsing with DI water follows for removal of the microgels that are not bound to the Au-coated substrate. Spin-coating can be considered a standardized method producing reproducible results in terms of the layer thickness and homogeneity of the film. However, the size consistency of the sensor is a challenge due to the uncontrolled spreading of the aliquot based on the spinning velocity. Hence, creating etalons in a millimeter and/or smaller scale is not feasible with these two methods.

To overcome these limitations, this study introduces an inkjet-printing-based approach for microgel deposition, offering digital control over droplet deposition, enabling reproducible sensor fabrication with higher consistency in microgel layer thickness, spatial patterning, and overall uniformity. A novel and highly precise method for fabricating etalon sensors at microscale dimensions.

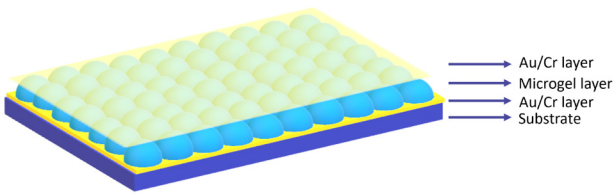

FIG. 1. Microgel-based etalon schematic.

Precisely controlling the dimensions of these sensors through inkjet printing technology will open new avenues for real-time monitoring of biological processes with high precision and sensitivity within microscale systems. Several methods have been used to deposit inks on substrates with spray coating,[19,20] stencil printing,[21] and inkjet printing[22] being among the well-established options. Spray coating forces the ink through a nozzle creating a fine aerosol.[23] No limitation on the rheological properties of the ink[19] makes spray coating a potential candidate for ink deposition. The main disadvantages of this method are the non-uniformity and the higher thickness of the formed film,[23,24] which in the microgel-based etalons are two main characteristics that should be controlled. The use of stencils to control the dimensions of the ink add further complexity leading to the waste of the material sprayed on the stencil area.[25] In stencil printing, the ink is deposited precisely in the apertures, preventing waste of the material, though requirement of mesh to maintain the stencil steady and the removal of the stencil directly impacts the print quality.[26,27]

Inkjet printing methods have attracted attention due to no materials wastage, and its direct and precise patterning with a resolution of 20–30 μm, counter to spin-coating and other conventional methods.[28] The production and deposition of ink droplets in the range of picoliters render it a cost-efficient process, which has been frequently used in the pharmaceutical industries for drugs, proteins, and nanoparticles deposition.[29,30] Inkjet printing enables digital control over the deposition process, offering flexibility in pattern design and customization, while its non-contact nature minimizes the risk of substrate damage and allows for printing on delicate or irregular surfaces, e.g., small cavities.[31] The most common technique for generating the droplets is the so-called "Drop-on-Demand" method in which ink droplets are ejected from the printer's nozzles only when necessary. A piezoelectric transducer creates a driving mechanism, which provides enough energy to form a drop of the used fluid.[22,31] All the above characteristics render inkjet printing the best candidate for microgel deposition on the Au-coated substrate, enabling reproducible sensor fabrication at millimeter or sub-millimeter scale, a critical feature for integration into microfluidic devices.

In this work, thermo-responsive pNIPAm-based microgels are rendered pH-responsive with the addition of acrylic acid (AAc) as a comonomer.[32,33] pNIPAm-co-AAc suspensions were studied as inks for inkjet-printed deposition on a Au-coated substrate. To meet the conditions required for inkjet-printing, namely, viscosity, surface tension, type, mixture, pH, and stability of the fluid,[34] surfactants were added to the initial suspension and their effect on surface tension, rheological properties, and particle size of the initial suspension was studied. After fully characterizing the ink's properties, inkjet-printing was performed demonstrating the feasibility of precise microgel deposition, leading to the formation of a 3 mm cohesive drop. Scanning electron microscopy (SEM) imaging confirmed the formation of a uniform monolithic microgel layer. Functionalization of the microgel-based etalons with 3-aminophenylboronic acid (APBA) enables microgels responsivity to glucose concentrations.[13] The response of the inkjet-printed sensors to temperature and glucose concentrations was tested via reflectance spectroscopy. From the reflectance spectra, the efficient response to the stimuli was observed. Atomic force microscopy (AFM) in liquid establishes a

better understanding of the swelling dynamics of the inkjet-printed microgels response to glucose concentrations. Controlled deposition of the microgels on Au-coated substrate with precise dimensions and high sensitivity to the stimuli offers promising capabilities for real-time monitoring of biological processes within microscale systems, with the potential for integration into organ-on-chip platforms and point-of-care diagnostics, highlighting their impact on next-generation biomedical sensing through advanced precision, scalability, and sensor miniaturization compared to traditional fabrication techniques.

II. EXPERIMENTS

A. Chemicals

Sodium dodecyl sulfate (SDS) (ACS reagent, $\geq 99.0\%$), hexadecyltrimethylammonium bromide (CTAB) ($\geq 99.0\%$), triton X-114 (TRT) (laboratory grade), sodium chloride (NaCl) (ACS reagent, $\geq 99.0\%$), α-D-glucose (ACS reagent), and APBA hydrochloride (98%) were obtained from Sigma-Aldrich, The Netherlands. 1-ethyl-3-(3-dimethylaminopropyl)carbodiimide hydrochloride (EDC), phosphate buffered saline [PBS (10×), pH 7.2], and BupH 2-(*N*-morpholino)ethanesulfonic acid (MES) buffered saline packets were obtained from Thermo Fisher Scientific Inc., The Netherlands, and were used as received or according to the package instructions. All de-ionized (DI) water had a resistivity of 18.2 M Ωcm and was obtained from a Milli-Q Type 1 system from Merck KGaA, Germany.

B. Ink preparation

A microgel suspension of pNIPAm-co-AAc with initial concentration 47.9 mg/ml was used. The microgel suspension was diluted with Milli-Q water to decrease the concentration to 42.6 mg/ml (further dilution was eschewed to avoid the coffee ring effect[17]). Dilution of the initial suspension with SDS, CTAB, and TRT surfactants at their Critical Micelle Concentration (CMC)[35,36] took place, leading to an end concentration of 42.6 mg/ml. The CMC level of the surfactants, their charge, and the volume added to the suspension are presented in Table I.

C. Surface tension

To define the suitability of the diluted suspensions as inks, surface tension measurements were performed. This measurement was performed on the OCA25 contact angle instrument (Dataphysics, Germany), using SCA202 V.5.0.41 version of the software. The pendant drop method was applied and the surface tension of the formed droplet was measured in its maximum volume before it detaches from the needle. The measurements were performed at a range of temperatures from 20 to 40 °C, which was controlled by a syringe heating device (SHD, Dataphysics, Germany) with an accuracy of ±0.1 °C, throughout the measurements. The sensitivity of the surface tension is 0.01 mN/m, and the experimental errors are less than 1.0 mN/m. Each measurement is performed three times.

TABLE I. Characteristics of the surfactant solutions used to dilute the initial microgel suspension.

Surfactant	Charge	CMC (mM)	Volume (μl)
SDS	Anionic	8	22.8
CTAB	Cationic	0.92	6.7
TRT	Non-ionic	0.23	4.7

D. Viscosity

The rheological behavior of the studied suspensions were determined by the Modular Compact Rheometer MCR 302 (Anton Paar, Austria) with a measuring parallel plate of 25 mm diameter PP25/P2 (Anton Paar, Austria) at a height of 0.145 mm. Each measurement consisted of an exponential increase of the shear rate (ramp up) from 10 to 10 000 (s^{-1}) followed by an exponential decrease in the shear rate (ramp down) from 10 000 to 10 (s^{-1}).[37] The measurements were performed at 20, 30, and 35 °C with an accuracy of ±0.1 °C, in a total of three times for each liquid.

E. Particle size

To evaluate the probability of clogging the inkjet nozzles[38] due to the microgel beads in the suspension, Dynamic Light Scattering (DLS) was used to measure the particle size of the beads. The Zetasizer Nano ZS and a ZEN0112 cuvette (Malvern Panalytical, UK) were used. To conduct these measurements, a volume fraction of 0.25% of the diluted suspensions and Milli-Q water was used. The particle size of the microgel beads was measured in the temperature range from 20 to 40 °C with an accuracy of ±0.1 °C. Each measurement was performed three times.

F. Inkjet printing

The printability of the diluted suspension was tested using the inkjet printer LP50 PiXDRO (SUSS MicroTec, Germany) with PIX-DRO 4.4.8.4 software. The cartridge was a Dimatix Materials Cartridge–Samba Cartridge (DMC Samba) (Fujifilm, Japan). The ideal fluid requirements provided by the company are presented in Table II,[34] and the diameter of the nozzle was measured to be 23.25 μm (see supplementary material section "Preparation of the ink," Fig. S1). Based on the surface tension, viscosity and particle size measurements and the appropriate range provided by the Dimatix, a diluted pNIPAm-co-AAc suspension with TRT was tested that approaches these ideal requirements. To deposit

TABLE II. Ideal fluid requirements for Dimatix® Materials Cartridge–Samba® Cartridge.

Property	Value
Viscosity	4–8 cps
Surface tension	28–32 dynes/cm
Type	Water based, solvent based
Mixture	Homogeneous, sub-micrometer particle size
pH	Neutral
Stability	Thermally stable for 2 weeks at 60 °C

pNIPAm-co-AAc-TRT on a gold glass substrate, the settings of the printer were adjusted. In particular, the waveform was defined by two pulses where the first pulse had voltage 38.8 mV, pulse width 2.2 μs, and pulse space 4.5 μs and the second pulse had voltage 10.0 mV, pulse width of 3.2 μs and pulse space of 4.5 μs. Printing was unidirectional where the substrate bed moves and the printhead stays still. The temperature of the substrate bed stays on default (22 °C), while the printhead temperature was set to 33 °C, enabling the jetting of the drops. The velocity and volume of the drop were determined by the software and have values of 5.70 m/s and 3.0 pl, respectively, at 33 °C of the printhead (see supplementary material section "Preparation of the ink," Fig. S2). To print a uniform 3 mm dot, attempts with several Dots-Per-Inch (DPI) were made. The DPI values of 1500 and 4000 were studied. The number of iterations was kept at one, while for the 1500 DPI, an attempt of two iterations was also made.

G. Microgel-based etalon fabrication

The fabrication process of the microgel-based etalon structure follows a similar procedure to previously published methods.[12,32] A layer of 2 nm chromium (Cr) and 15 nm gold (Au) was deposited on glass coverslips of 18 × 18 mm^2 (Menzel-Gläser, Germany) using thermal physical vapor deposition (PVD) (CHA Industries, Inc., Solution PLC-S7) at a speed of 1 and 3 Å s^{-1}, respectively. pNIPAm-co-AAc-TRT microgels were deposited on the Au layer by the LP50 PiXDRO inkjet printer (SUSS MicroTec, Germany), forming a uniform film (see Sec. III B). The printed samples were dried on a hotplate at 30 °C for 1 h and rinsed with Milli-Q water to remove excess microgels not bound to the Au layer. The samples were dried overnight on a hotplate at 30 °C and subsequently, a top layer of 2 nm Cr and 15 nm Au was evaporated on the microgel film, creating the etalon structure in a shape of circle with 3 mm diameter. In the case of two iterations (1500 DPI, see Sec. III B), the first layer of microgels was printed on the gold substrate, dried on a hotplate at 30 °C for 1 h, and the excess material was rinsed. A second print over the same spot took place, and the same procedure was being followed.

The inkjet-printed microgels were functionalized with APBA to render them responsive to glucose, following a procedure similar to Sorrell *et al.*[13] In summary, the microgel-based etalon samples were immersed in pH 4.7 MES buffered saline, to which 9 mg of APBA was added, and the mixture was stirred on a magnetic stirrer at room temperature for 1 h. 20 mg of EDC was added and stirred until fully dissolved, followed by 5 h of refrigeration. Additional 4.5 mg of APBA per sample was added to the solution and stirred for 30 m, followed by the addition of 20 mg of EDC per sample and overnight reaction at 4 °C. The samples were then rinsed with de-ionized water and soaked in 10 mM PBS buffer (with 150 mM ionic strength from NaCl) at pH 7.2 for 2 h to remove unreacted reagents. Noteworthily, since the APBA molecule is added after microgel printing as a post-processing step, its presence does not affect the printability of microgel ink and/or the printing process.

H. Microscopy imaging

Microscopy images of the monolithic layer of the printed microgels were taken with a JSM-6010LA (JEOL, Ltd, Japan) scanning electron microscope (SEM) using INTOUCHSCOPE 1.12 software. An optical microscope Nanoro M (LIG Nanowise, UK) was used to define the print quality.

I. Reflectance spectroscopy

Detection of the microgels response to the stimuli of interest was performed. The microgel-based etalon was placed in a glass Petri dish and a UV/vis reflectance probe (Ocean Optics, SR2 UV-VIS, Florida) was placed on top of the etalon surface in adjusted distance for optimal signal. To maintain consistency of the recorded spectra, the probe remains at the same position throughout each set of experiments. The tested liquids were 1 mM DI water/NaCl of pH 6.5 and glucose concentration (C_g) of 0–100 mg/dl. Once the etalon was immersed in the studied liquids, a spectrum was recorded by OCEAN VIEW 2.0.14 software with a wavelength range of 400–1000 nm. The temperature range of the liquid was from 20 to 65 °C, controlled by heating the glass Petri dish up to the desired temperature using a hot plate to maintain steady temperature of the liquid. Reflectance spectra were recorded in total of three times for each liquid and temperature.

J. In-liquid atomic force microscopy (AFM)

To understand the swelling dynamics of the inkjet-printed microgels in response to glucose concentration in-liquid, AFM was used (Brüker Nanowizard BioAFM equipped with a ScanAsyst-fluid probe; the properties of the probe are described in Table III). A droplet of solution was placed on the sample, after which the probe was brought into contact with the sample. The set-point (maximum force on the surface) was 5 nN. A 5 × 5 μm^2 area was scanned in Quantitative Imaging (QI)-mode imaging and height profiles were extracted. Processing of the images was performed in the JPK data processing software (v8.0). A plane fit and line leveling were applied, using a linear fitting procedure provided in the software, with default settings. Liquids of pH 6.5 and glucose concentrations of 20, 40, and 80 mg/dl were studied. In each liquid, a different inkjet-printed etalon of 4000 DPI was used, and the measurements were performed three times at each condition.

III. RESULTS AND DISCUSSION

A. Ink characterization

The ability to precisely control the dimensions of a microgel-based etalon sensor offers new possibilities to organ-on-chip applications. Inkjet printing is a valuable tool to achieve this outcome. For this purpose, the properties of the tested ink should be in line with the requirements of inkjet printer. Hence, adjustments not only on the printer but also on the initial pNIPAm-based

TABLE III. Properties of ScanAsyst-fluid probe.

Property	Value
Nominal tip radius	20 nm
Cantilever length	70 μm
Cantilever width	10 μm
Spring constant	0.4 N/m

suspension are made. The pNIPAm-co-AAc suspension was used to fabricate microgel-based etalon sensors responsive to temperature and pH. The properties of the suspensions, namely, surface tension, viscosity, and the particle size of both the initial and the diluted, with surfactants, samples are studied.

1. Surface tension

To study the effect of added surfactants to the surface tension of the microgel suspensions, density measurements were initially performed for all the studied samples in a temperature range of 20–40 °C (see supplementary material section "Preparation of the ink," Fig. S3). The obtained density values were used during the surface tension experiments. In Fig. 2, the plot of surface tension as a function of temperature is presented. It was observed that the surface tension of pNIPAm-co-AAc suspension without the addition of any surfactant was 67.44 ± 0.67 mN/m at 20 °C. A slight decrease of this value was obtained with increase in temperature, though still far exceeds the required range for printing (28–32 dynes/cm, Table III). The addition of surfactants had a noticeable effect on the surface tension of the initial suspension, leading to a decrease of roughly 35%. An immense decrease of the surface tension was observed with the addition of TRT at the CMC level, leading to a value of 38.40 ± 0.86 mN/m at 20 °C with a further decrease at higher temperatures. The addition of TRT leads to values close to the required range for printable ink.

2. Viscosity

The suitability of using the pNIPAm-based suspensions as ink in the printer depends on both their rheological behavior and viscosity values at high shear rate, given that shear rates can reach above 300 000 s^{-1}.[22,34] In Fig. 3, the logarithmic plot of viscosity of the diluted suspensions as a function of shear rate is presented for three different temperatures (20, 30, and 35 °C). All the studied suspensions behaved as non-Newtonian shear thinning fluids, presenting a pseudo-newtonian behavior at high shear rates (> 1000 s^{-1}). The asymptotic viscosity (μ_∞) of the studied suspensions in high shear rates and at three different temperatures are provided in Table IV. At 20 °C, only the pNIPAm-based suspensions with added TRT and CTAB were within the appropriate range (4–8 cps, Table III). As the temperature increases, the viscosity is decreasing leading to values lower than the range provided by Dimatix. This suggests that printing at temperatures higher than room temperature may lead to limitations for microgel deposition. However, the temperature must remain below the microgel's lower critical solution temperature (LCST), at approximately 32 °C,[7] to prevent de-swelling, which would compromise its functional properties during deposition. All the studied samples exhibited behavior appropriate for printing at high shear rates, but based on the viscosity values, the diluted suspensions with TRT and CTAB were more prominent candidates as inks.

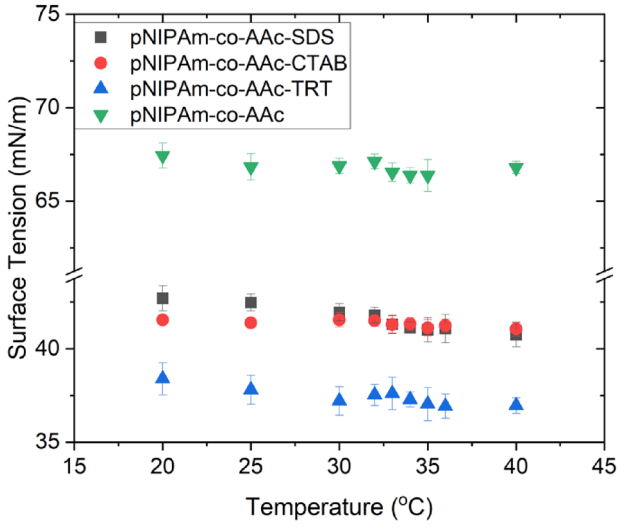

FIG. 2. Surface tension as a function of temperature for the diluted suspensions (C = 42.6 mg/ml) with DI water (green downward triangles), SDS (black squares), CTAB (red circles), and TRT (blue upwards triangles). Surface tension values for all the studied liquids present standard deviation of ±0.2 to ±0.9 mN/m. Each measurement is performed three times.

3. Particle size

The response of thermo-responsive pNIPAm-based microgels to temperature has been extensively studied.[7,39,40] A volume phase transition is observed when the temperature of the solvent reaches the LCST. Below the LCST, the microgels are in the swollen state while repulsion of water above the LCST leads to a de-swollen (shrunken) state of the microgel beads.[7,39] Figure 4 shows that at 20 °C, in their swollen state, pNIPAm-co-AAc microgels had a size of 924 ± 18 nm. An immense decrease was observed above LCST reaching to 477 ± 16 nm at 40 °C. The addition of surfactants in the initial suspension had a minimal influence on the size of the beads, leading to the assumption that the surfactants were not accumulating on the surface of the microgel beads and that the micelles formed at the CMC level were diffused in the solvent, provoking decrease of the surface tension of the liquid. At temperatures above 25 °C, the effective size of the microgel beads was in sub-micrometer scale, with range of 30–50 times smaller than the nozzle diameter, proving that clogging of the nozzles of the cartridge can be prevented.[41]

B. Inkjet-printed etalon sensor

Based on the results from ink characterization [(1) surface tension, (2) viscosity, and (3) particle size], the pNIPAm-co-AAc-TRT suspension was used as the ink since its properties are approaching the ranges set by Dimatix. In Fig. 5(a), the optical microscopy image of the sample printed with 1500 DPI in one iteration is presented. Reproducibility of printing at 1500 DPI was achieved [see supplementary material section "Inkjet-printed sensor," Figs. S4(a) and S4(b)]. However, with 1500 DPI, the formation of cohesive drop was not obtained, leading to uncovered areas. Notably, the SEM image [Fig. 5(b)] shows the formation of a monolithic microgel layer on the gold substrate. An attempt with 1500 DPI and two iterations improved the quality of the print by decreasing the uncovered areas [Fig. 6(a)]. The SEM imaging [Fig. 6(b)] revealed that two separate prints were performed, creating a hill like structure. Hence, the monolithic layer

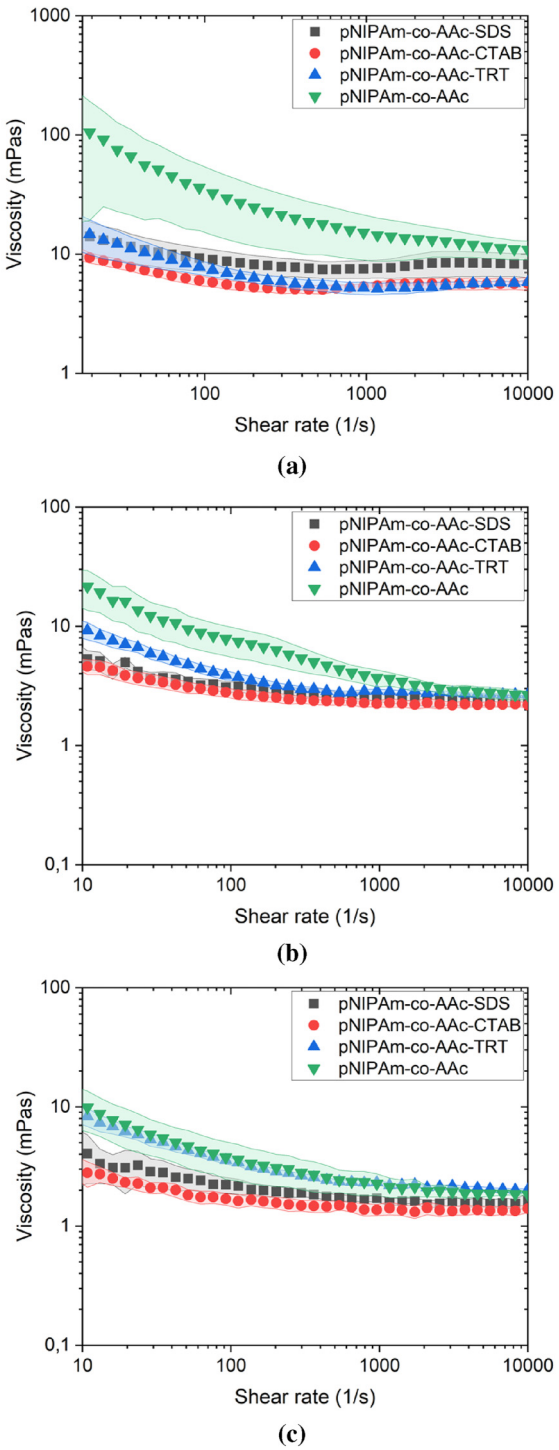

FIG. 3. The logarithmic plot of viscosity as a function of the shear rate for the diluted suspensions with SDS, CTAB, TRT, and DI water at (a) 20, (b) 30, and (c) 35 °C, included shaded error bars (±0.03 to ±1.9 mPa s). Each measurement is performed three times.

TABLE IV. The asymptotic viscosity of the diluted suspensions with SDS, CTAB, TRT, and DI water at 10 000 s^{-1} and at 20, 30, and 35 °C.

Sample	Asymptotic viscosity at 20 °C (mPa s)	Asymptotic viscosity at 30 °C (mPa s)	Asymptotic viscosity at 35 °C (mPa s)
pNIPAm-co-AAc	10.9 ± 1.9	2.7 ± 0.2	1.2 ± 0.03
pNIPAm-co-AAc-SDS	8.2 ± 1.8	2.4 ± 0.2	1.6 ± 0.3
pNIPAm-co-AAc-CTAB	5.7 ± 0.7	2.2 ± 0.1	1.4 ± 0.1
pNIPAm-co-AAc-TRT	5.8 ± 0.2	2.7 ± 0.1	2.0 ± 0.1

was not uniform throughout the sample. Increase of the DPI to 4000 led to the formation of a 3 mm cohesive drop [Fig. 7(a)], showing consistency and reproducibility among the several printed samples [see supplementary material section "Inkjet-printed sensor," Figs. S5(a)–S5(c)]. The SEM image [Fig. 7(b)] confirmed the formation of a uniform monolithic microgel layer, rendering it a possible candidate for sensing applications.

C. Reflectance spectroscopy

Having achieved the fabrication of an inkjet-printed 3 mm microgel-based etalon, reflectance spectroscopy was performed to study microgel's response (swelling/de-swelling) to the stimuli. The swelling/de-swelling behavior of the microgels to glucose concentration and temperature changes result in an increase/decrease in the distance between the two gold layers, leading to a peak shift in the wavelength, which was successfully detected by reflectance spectroscopy.

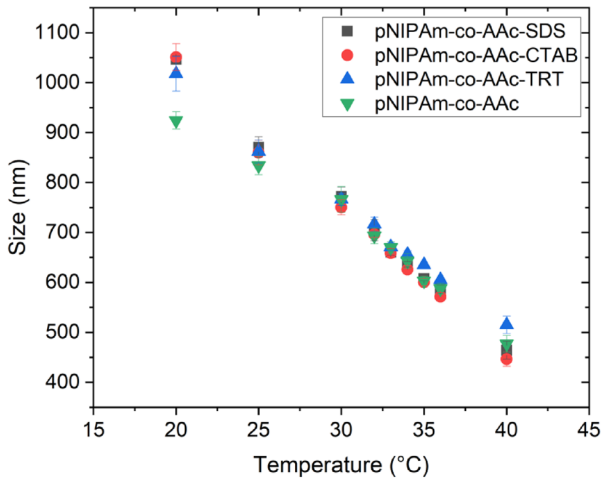

FIG. 4. Particle size of the diluted suspensions with SDS, CTAB, TRT, and DI water as a function of temperature. The particle size of all the studied liquids presents standard deviation of ±4 to ±35 nm, with a total of three measurements at each temperature.

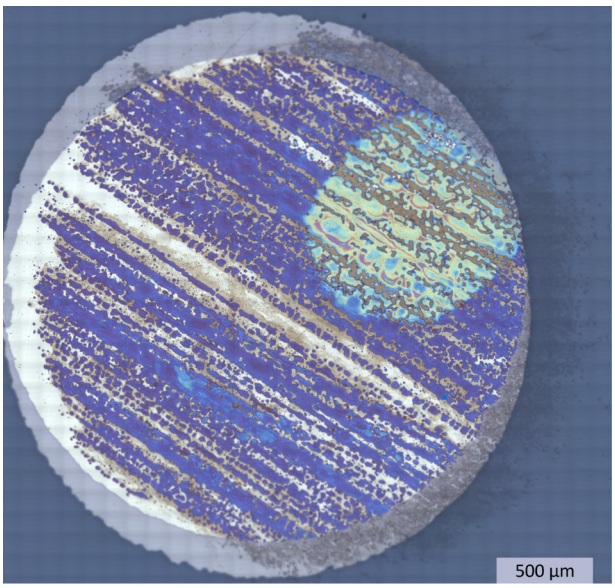

(a)

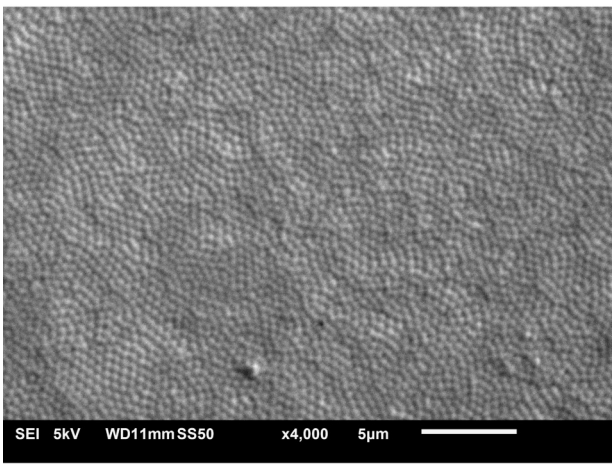

(b)

FIG. 5. (a) Optical microscopy and (b) SEM images of the printed pNIPAm-co-AAc-TRT sample with one iteration at a DPI of 1500.

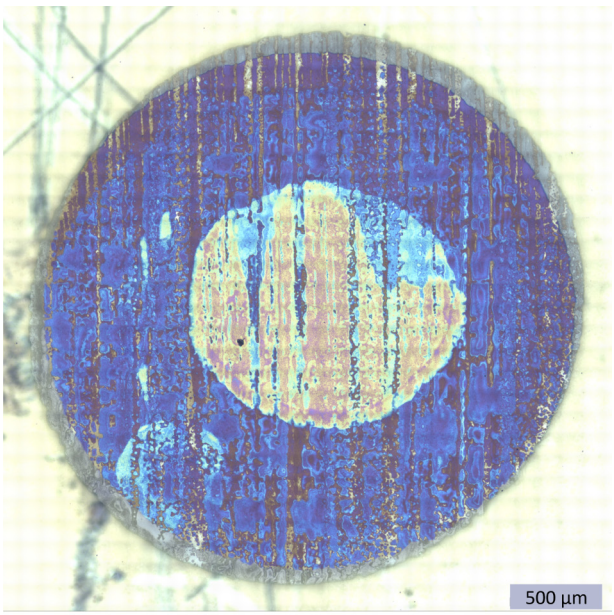

(a)

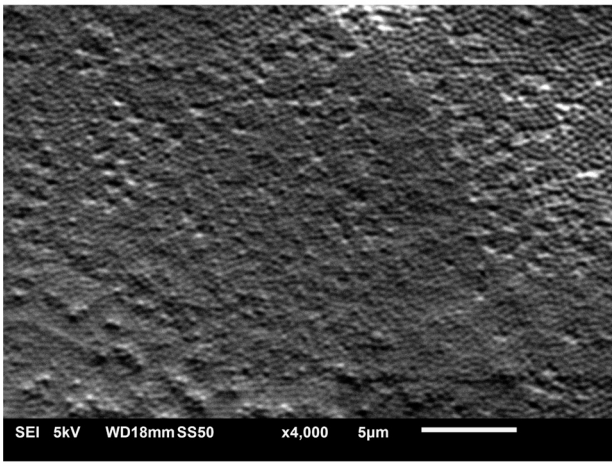

(b)

FIG. 6. (a) Optical microscopy and (b) SEM images of the printed pNIPAm-co-AAc-TRT sample with two iterations at a DPI of 1500.

1. Temperature

The reflectance spectra and the peak shift for different temperatures of the 4000 DPI print are presented in Fig. 8. A blue shift in the reflectance spectrum was observed with increase of the temperature from 22 to 45 °C at pH 6.5, indicating the de-swelling behavior of the beads. For reproducibility purposes, each experiment was performed three times. A typical reflectance spectrum is presented in Fig. 8(a). At temperatures from 45 to 65 °C, no further shift of the wavelength was observed indicating that the beads have reached the most de-swollen state at around 45 °C and further increase of temperature did not provoke decrease in the size of the microgels. The average peak shift of the three measurements is shown in Fig. 8(b).

Similar de-swollen behavior of the microgel beads with the temperature was observed for the samples of 1500 DPI with one and two iterations [see supplementary material section "Reflectance spectroscopy," Figs. S6(a), S6(b), S7(a), and S7(b)]. The formation of a cohesive drop with 4000 DPI leads to monolithic layer of microgel throughout the sample area. However, with 1500 DPI, the

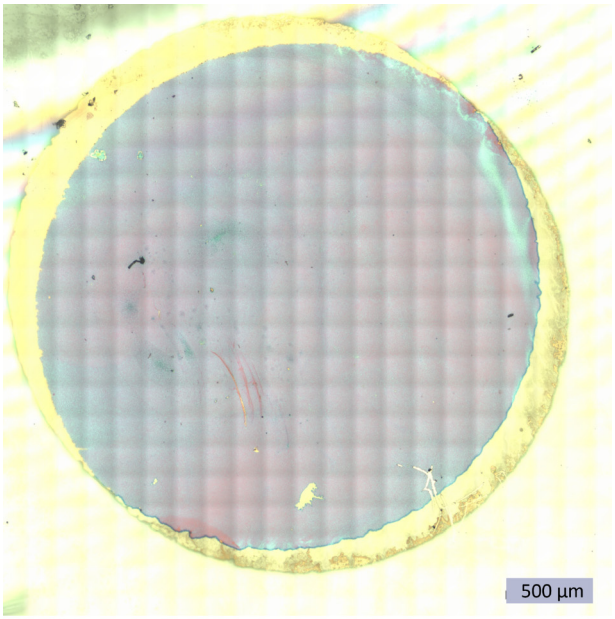

(a)

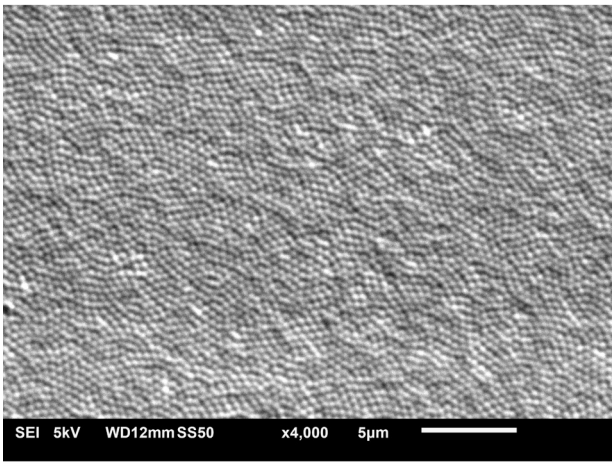

(b)

FIG. 7. (a) Optical microscopy and (b) SEM images of the printed pNIPAm-co-AAc-TRT sample with one iteration at a DPI of 4000.

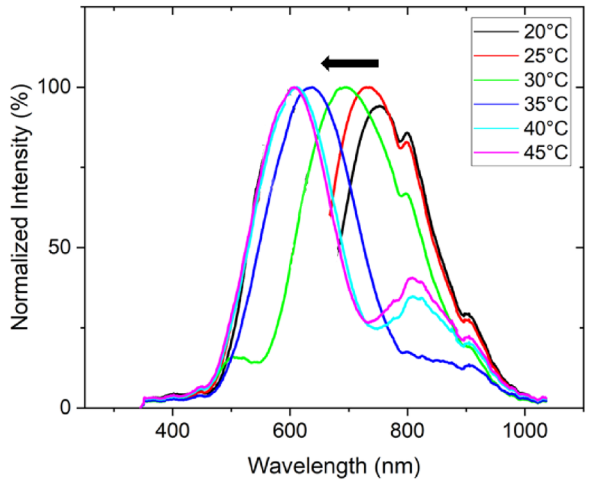

(a)

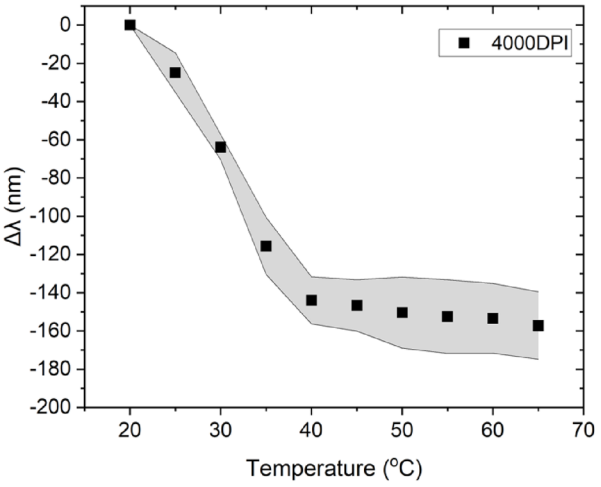

(b)

FIG. 8. (a) Typical reflectance spectrum and (b) average peak shift of the printed pNIPAm-co-AAc-TRT microgel-based etalon sensor at 4000 DPI in different temperatures at pH 6.5 (shaded region shows the standard deviation obtained from three data points for each temperature). The negative values of $\Delta\lambda$ in plot (b) demonstrate the blue shift due to the de-swelling of the microgels with increase in temperature, with $\Delta\lambda = \lambda_{\text{testcondition}} - \lambda_{\text{pH6.5,22°C}}$.

monolithic layer has discrepancies due to the uncovered areas, for the samples of one iteration, and the hilly areas, for the samples of two iterations. This creates samples with different initial thickness of the microgel layer based on the DPI and the iterations leading to different absolute values of the wavelength in the reflectance spectra [see supplementary material section "Reflectance spectroscopy," Figs. S6(a) and S6(b)]. The results indicate that the inkjet-printed microgel-based etalon sensors can effectively respond to temperature for all the tested samples.

2. Glucose

Reflectance spectroscopy measurements were performed for the inkjet-printed samples functionalized with APBA to examine their response to glucose concentrations. Glucose buffer solutions were prepared with pH 6.5 (1 mM DI water/NaCl) and glucose concentration (C_g) of 10–100 mg/dl. All the experiments were performed at 22 °C. A red shift was observed in reflectance spectra in all the glucose concentrations for all the studied DPIs, proving the swelling behavior of the microgel beads. Each experiment was performed

three times. In Fig. 9, the typical reflectance spectrum and the average peak shift of the 4000 DPI sample are presented, showing the sensitivity of APBA-functionalized microgels to glucose concentrations up to 100 mg/dl. In $C_g > 60$ mg/dl, the peak shift was not that distinct pointing out that APBA-functionalized microgels were reaching a saturation point, where no more glucose molecules can bind to. The number of APBA molecules that binds to the pNIPAm-co-AAc microgels depends on the surface area of the sensor. The sensitivity of the APBA-functionalized etalons to glucose relies on the reversible binding of diol-containing glucose molecules to hydroxylated APBA groups.[13,18] Thus, the sensitivity of microgel-based etalon sensors to glucose is closely linked to the number of APBA moieties available for binding. Hence, by decreasing the size of the etalon sensor, its glucose sensitivity is expected to decrease. In the samples of 1500 DPI, the saturation point was reached at $C_g = 60$ mg/dl [see supplementary material section "Reflectance spectroscopy," Figs. S8(a), S8(b), S9(a), and S9(b)]. The formation of a monolithic layer of microgels on the substrate, achieved with 4000 DPI, favors the binding of APBA molecules to the AAc groups of the beads, ensuring greater uniformity in the sensor response and lower standard deviations compared to the 1500 DPI samples. The performance of the APBA-functionalized inkjet-printed microgel-based etalons could render them a potential candidate for *in situ* sensors in organ-on-chip applications for the detection of glucose levels encountered in specialized cell culture environments, such as neuronal or stem cell cultures, where glucose levels are often maintained within the range of 40–100 mg/dl.[42,43]

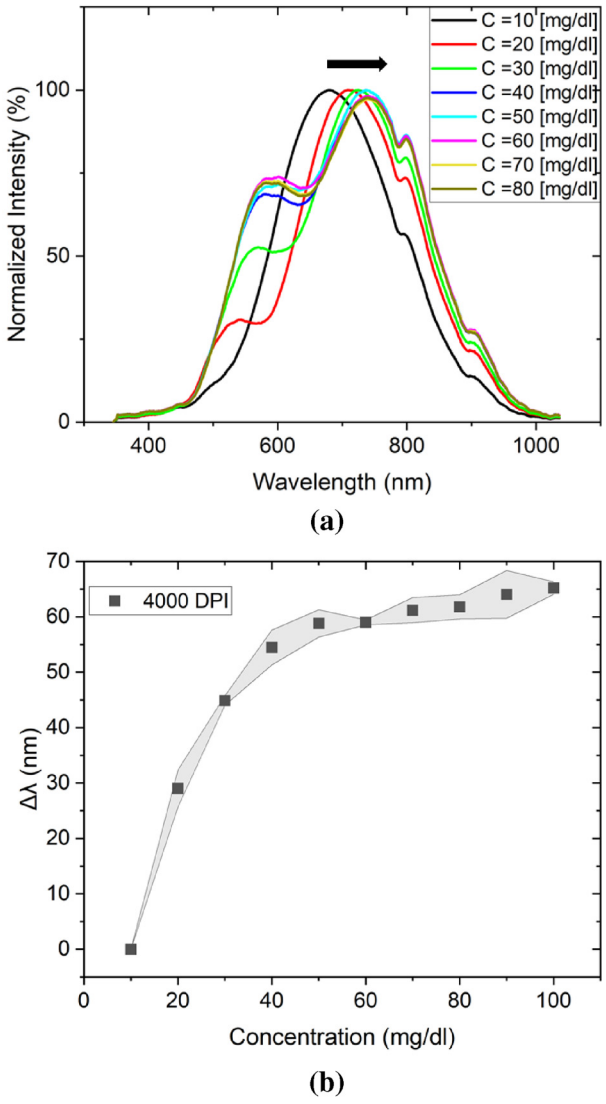

FIG. 9. (a) Typical reflectance spectrum and (b) average peak shift of the 4000 DPI pNIPAm-co-AAc-TRT microgel-based etalon sensor in different glucose concentrations at 22 °C and pH 6.5 (shaded region shows the standard deviation obtained from three data points for each glucose concentration). The positive values of $\Delta\lambda$ in plot (b) demonstrate the red shift due to the swelling of the microgels with an increase of glucose concentration, with $\Delta\lambda = \lambda_{testcondition} - \lambda_{pH6.5,22^{\circ}C}$.

3. In-liquid AFM

The swelling dynamics of the microgels were tested by immersing the 4000 DPI microgel-based etalons in glucose buffer solutions of pH 6.5 with concentrations of 20, 40, and 80 mg/dl. In Fig. 10, the thickness of the microgel layer is presented as a function of time. An increase of 20% in size was observed for the microgels in all the tested glucose concentrations in a span of 2 h. The plot can be divided into three sections based on the response of the beads to the stimuli. An immediate response of the microgel beads to the stimuli was observed, presenting a sharp slope ($n = 1.45$) in the first 40 min (Sec. I). In particular, when

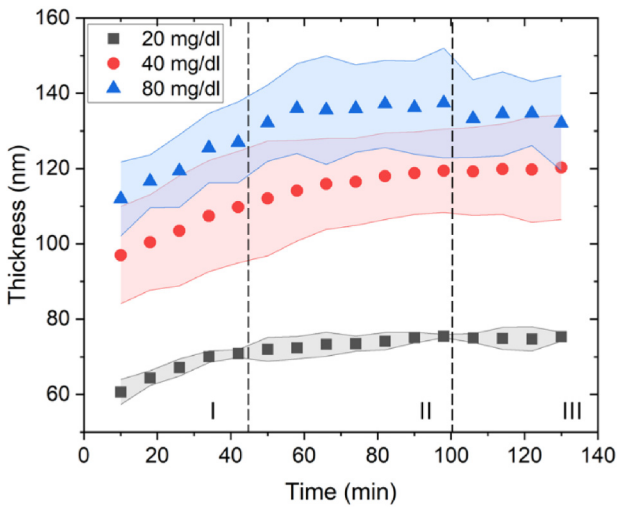

FIG. 10. Thickness of the microgel layer on the 4000 DPI microgel-based etalon vs time, when immersed in glucose buffer solutions (pH 6.5) in concentrations of 20, 40, and 80 mg/dl. Sections I, II, and III correspond to the dynamic response of the microgels to the stimuli. The high rate observed in Sec. I decrease in the rate observed in Sec. II and reaching a steady state in Sec. III.

immersed in the solution with $C_g = 20$ mg/dl, the slope attended was $n_{20} = 0.33$ while for $C_g = 40$ mg/dl and $C_g = 80$ mg/dl, it was $n_{40} = 0.41$ and $n_{80} = 0.49$ showing that the response was more prominent with the increase of the glucose concentration in the solution. The swelling rate of the beads decreased in the span of 40–106 min ($n_{20} = 0.08$, $n_{40} = 0.15$, and $n_{80} = 0.08$, Sec. II). The steady state of the beads was reached after 106 min ($n_{20} = 0.01$, $n_{40} = 0.04$, and $n_{80} = 0.04$, Sec. III). The thickness of the microgel layer was increased by increasing the glucose concentration where at the steady state for 20 mg/dl, the average thickness was $t_{20} = 75.0 \pm 1.2$ nm and for 80 mg/dl, $t_{80} = 134.6 \pm 8.5$ nm, which was justified by the swollen behavior of the microgels as a response to glucose. The formation of a closely packed monolithic microgel layer on the gold-coated substrate leads to thickness values on the range of 75–135 nm, notably smaller than the initial size of the microgel beads in the suspension (Fig. 4), as a result of changes in the interfacial properties.[7,44]

IV. CONCLUSIONS

In this study, we successfully demonstrate the characterization and the use of pNIPAm-based suspensions as inks for inkjet-printing, making the fabrication of inkjet-printed microgel-based etalon sensors feasible using this technique. Through characterization of the microgel (pNIPAm-co-AAc) suspensions, we optimized the properties of the suspensions to meet the requirements of the ink for inkjet printing, focusing on surface tension, viscosity, and particle size. By incorporating surfactants into the pNIPAm-co-AAc suspension, we effectively reduced surface tension, enhancing printability and ensuring consistency in ink behavior at different temperatures. At high shear rates, in which inkjet-printer operates, the suspensions exhibit pseudo-Newtonian behavior suitable for printing. This represents a significant advancement over traditional deposition techniques, offering a scalable and reproducible approach to sensor fabrication. Leveraging the precise control and the reproducibility offered by inkjet printing technology, we achieved uniform deposition of thermo-responsive pNIPAm-based microgels on Au-coated substrates with dimensions as small as 3 mm, showcasing high sensitivity to stimuli. The response of inkjet-printed microgel-based etalons to temperature and glucose concentrations were assessed through reflectance spectroscopy and in-liquid AFM. Our results demonstrate a distinct shift in the wavelength peak during reflectance spectroscopy experiments, indicating the swelling and de-swelling behavior of the microgels in response to temperature changes and glucose concentrations. AFM analysis revealed the dynamic swelling kinetics of the microgels in different glucose concentration solutions, further confirming their responsiveness to stimuli. These findings highlight the novelty of our inkjet-printing approach as a robust method for producing miniaturized, highly sensitive optical biosensors with precisely controlled geometry. Overall, the inkjet-printed microgel-based etalons offer promising capabilities for real-time monitoring of biological processes within microscale systems, particularly in organ-on-chip applications and point-of-care testing. The precise control over sensor dimensions and high sensitivity to stimuli make them potential candidates for *in situ* sensing of glucose levels, paving the way for advancements in personalized healthcare and disease diagnostics. Future work will focus on studying the selectivity of the sensor toward glucose in complex biological environments and assess the sensor's current limit of detection (LOD) to evaluate its suitability for real-time biochemical monitoring in tissue models and microphysiological systems. Further optimization of ink formulations and printing parameters could enhance the performance and applicability of these sensors in diverse biomedical and analytical fields.

SUPPLEMENTARY MATERIAL

Further details of the following experimental procedures along with additional figures and explanations can be found in the supplementary material. Preparation of the ink, with subsections of inkjet printing and density of pNIPAm-based suspensions, inkjet-printed sensor, and reflectance spectroscopy are included in the supplementary material.

ACKNOWLEDGMENTS

We wish to acknowledge Dr. Andres Hunt (Department of Precision and Microsystems Engineering, Faculty of Mechanical Engineering, Delft University of Technology (TUD), The Netherlands) for invaluable advice and help on Inkjet printing. We would also like to thank Dr. Mengmeng Zhang (Department of Process and Energy, Faculty of Mechanical Engineering, TUD , The Netherlands) for preparing the graphical abstract.

AUTHOR DECLARATIONS

Conflict of Interest

The authors have no conflicts to disclose.

Author Contributions

G. Kontaxi: Data curation (equal); Formal analysis (equal); Methodology (equal); Validation (equal); Visualization (equal); Writing – original draft (equal); Writing – review & editing (equal). **T. J. Lugtmeijer:** Data curation (lead); Formal analysis (lead); Validation (equal); Visualization (equal). **M. J. Serpe:** Supervision (supporting); Writing – review & editing (lead). **H. Bazyar:** Conceptualization (equal); Project administration (equal); Supervision (equal); Writing – review & editing (equal).

DATA AVAILABILITY

The data that support the findings of this study are openly available in 4TU repository at https://doi.org/10.4121/0d5f9f9a-a71e-4e30-9144-f239d48a9543, Ref. 45.

REFERENCES

[1]P. K. W. Mandy, L.Y. Sin, K. E. Mach and J. C. Liao, "Advances and challenges in biosensor-based diagnosis of infectious diseases," Expert. Rev. Mol. Diagn. **14**, 225–244 (2014).
[2]A. Haleem, M. Javaid, R. P. Singh, R. Suman, and S. Rab, "Biosensors applications in medical field: A brief review," Sens. Int. **2**, 100100 (2021).
[3]M. M. Honikel, C.-E. Lin, D. Probst, and J. La Belle, "Facilitating earlier diagnosis of cardiovascular disease through point-of-care biosensors: A review," Crit. Rev. Biomed. Eng. **46**, 53–82 (2018).
[4]E. Ferrari, C. Palma, S. Vesentini, P. Occhetta, and M. Rasponi, "Integrating biosensors in organs-on-chip devices: A perspective on current strategies to monitor microphysiological systems," Biosensors **10**(9), 110 (2020).

[5]T. Shu, L. Hu, Q. Shen, L. Jiang, Q. Zhang, and M. J. Serpe, "Stimuli-responsive polymer-based systems for diagnostic applications," J. Mater. Chem. B **8**, 7042–7061 (2020).
[6]L. Hu, T. Shu, Y. Wan, C. Fang, F. Gao, and M. J. Serpe, "Recent advances in stimuli-responsive polymers for sensing and actuation," Mol. Syst. Des. Eng. **6**, 108–121 (2021).
[7]S. Wellert, M. Richter, T. Hellweg, R. von Klitzing, and Y. Hertle, "Responsive microgels at surfaces and interfaces," Z. Phys. Chem. **229**, 1225–1250 (2015).
[8]C. Ancla, V. Lapeyre, I. Gosse, B. Catargi, and V. Ravaine, "Designed glucose-responsive microgels with selective shrinking behavior," Langmuir **27**, 12693–12701 (2011).
[9]Q. M. Zhang, W. Xu, and M. J. Serpe, "Optical devices constructed from multi-responsive microgels," Angew. Chem. **126**, 4927–4931 (2014).
[10]C. L. Bayer and N. A. Peppas, "Advances in recognitive, conductive and responsive delivery systems," J. Controlled Release **132**, 216–221 (2008).
[11]S. Santhosh, M. Nanjan, and M. Chandrasekar, "Ovarian solid tumors: Current treatment and recent developments using stimuli-responsive polymers: A systemic review," J. Drug Delivery Sci. Technol. **51**, 621–628 (2019).
[12]Y. Gao, X. Li, and M. J. Serpe, "Stimuli-responsive microgel-based etalons for optical sensing," RSC Adv. **5**, 44074–44087 (2015).
[13]C. D. Sorrell and M. J. Serpe, "Glucose sensitive poly (N-isopropylacrylamide) microgel based etalons," Anal. Bioanal. Chem. **402**, 2385–2393 (2012).
[14]M. R. Islam and M. J. Serpe, "Label-free detection of low protein concentration in solution using a novel colorimetric assay," Biosens. Bioelectron. **49**, 133–138 (2013).
[15]G. Brooker, *Modern Classical Optics*, Oxford Master Series in Physics (Oxford University Press, Oxford, New York, 2003), Vol. 8, oCLC: ocm52829216.
[16]M. Deetlefs, K. R. Seddon, and M. Shara, "Neoteric optical media for refractive index determination of gems and minerals," New J. Chem. **30**, 317 (2006).
[17]C. D. Sorrell, M. C. D. Carter, and M. J. Serpe, "A "paint-on" protocol for the facile assembly of uniform microgel coatings for color tunable etalon fabrication," ACS Appl. Mater. Interfaces **3**, 1140–1147 (2011).
[18]G. Kontaxi, G. Wensink, P. Sberna, M. Rücker, V. Garbin, M. Serpe, and H. Bazyar, "Microgel-based etalon membranes: Characterization and properties," APL Mater. **12**, 091113 (2024).
[19]F. Aziz and A. Ismail, "Spray coating methods for polymer solar cells fabrication: A review," Mater. Sci. Semicond. Process. **39**, 416–425 (2015).
[20]T. Carey, C. Jones, F. Le Moal, D. Deganello, and F. Torrisi, "Spray-coating thin films on three-dimensional surfaces for a semitransparent capacitive-touch device," ACS Appl. Mater. Interfaces **10**, 19948–19956 (2018).
[21]H. Wickström, R. Koppolu, E. Mäkilä, M. Toivakka, and N. Sandler, "Stencil printing—A novel manufacturing platform for orodispersible discs," Pharmaceutics **12**, 33 (2020).
[22]B. Derby and N. Reis, "Inkjet printing of highly loaded particulate suspensions," MRS Bull. **28**, 815–818 (2003).
[23]F. C. Krebs, "Fabrication and processing of polymer solar cells: A review of printing and coating techniques," Solar Energy Mater. Solar Cells **93**, 394–412 (2009).
[24]C. Girotto, B. P. Rand, J. Genoe, and P. Heremans, "Exploring spray coating as a deposition technique for the fabrication of solution-processed solar cells," Solar Energy Mater. Solar Cells **93**, 454–458 (2009).
[25]R. Kay and M. Desmulliez, "A review of stencil printing for microelectronic packaging," Soldering Surface Mount Technol. **24**, 38–50 (2012).
[26]F. I. Indicatti, M. Rädler, F. Günter, E. Stammen, and K. Dilger, "Stencil printing of adhesive-based fuel cell sealings: The influence of rheology on bubble formation during the separation step," Proc. Inst. Mech. Eng., Part C **238**, 2552–2567 (2024).
[27]M. Rusdi, M. Abdullah, S. Chellvarajoo, M. Abdul Aziz, M. Abdullah, P. Rethinasamy, S. Veerasamy, and D. G. Santhanasamy, "Stencil printing process performance on various aperture size and optimization for lead-free solder paste," Int. J. Adv. Manuf. Technol. **102**, 3369–3379 (2019).
[28]S. H. Eom, H. Park, S. Mujawar, S. C. Yoon, S.-S. Kim, S.-I. Na, S.-J. Kang, D. Khim, D.-Y. Kim, and S.-H. Lee, "High efficiency polymer solar cells via sequential inkjet-printing of PEDOT:PSS and P3HT:PCBM inks with additives," Org. Electron. **11**, 1516–1522 (2010).
[29]B.-J. De Gans, P. C. Duineveld, and U. S. Schubert, "Inkjet printing of polymers: State of the art and future developments," Adv. Mater. **16**, 203–213 (2004).
[30]M. Singh, H. M. Haverinen, P. Dhagat, and G. E. Jabbour, "Inkjet printing—Process and its applications," Adv. Mater. **22**, 673–685 (2010).
[31]I. M. Hutchings and G. D. Martin, *Inkjet Technology for Digital Fabrication* (Wiley Online Library, 2013).
[32]C. D. Sorrell, M. C. Carter, and M. J. Serpe, "Color tunable poly (*N*-isopropylacrylamide)-*co*-acrylic acid microgel–Au hybrid assemblies," Adv. Funct. Mater. **21**, 425–433 (2011).
[33]K. Kratz, T. Hellweg, and W. Eimer, "Influence of charge density on the swelling of colloidal poly (*N*-isopropylacrylamide-co-acrylic acid) microgels," Colloids Surf. A: Physicochem. Eng. Asp. **170**, 137–149 (2000).
[34]See https://asset.fujifilm.com/www/us/files/2021-04/ae8a1e167ce8c273fcdd31ecffd9ec80/PDS00142.pdf for "Dimatix® Materials Cartridge - Samba® Cartridge" (2021).
[35]R. Banik, B. B. Mondal, R. Sardar, and S. Ghosh, "Comparative study of the aggregation behavior of some ionic surfactants with nonionic triton X-114 in water and a water/2,2,2-trifluoroethanol mixture," Ind. Eng. Chem. Res. **63**, 3057–3071 (2024).
[36]H. Bazyar, N. van de Beek, and R. G. Lammertink, "Liquid-infused membranes with oil-in-water emulsions," Langmuir **35**, 9513–9520 (2019).
[37]G. Ovarlez, "Introduction to the rheometry of complex suspensions," in *Understanding the Rheology of Concrete* (Elsevier, 2012), pp. 23–62.
[38]A. Marin, H. Lhuissier, M. Rossi, and C. J. Kähler, "Clogging in constricted suspension flows," Phys. Rev. E **97**, 021102 (2018).
[39]S. J. Lue, B.-W. Chen, C.-M. Shih, F.-Y. Chou, J.-Y. Lai, and W.-Y. Chiu, "Micron-and nano-sized poly (N-isopropylacrylamide-co-acrylic acid) latex syntheses and their applications for controlled drug release," J. Nanosci. Nanotechnol. **13**, 5305–5315 (2013).
[40]L. D. Taylor and L. D. Cerankowski, "Preparation of films exhibiting a balanced temperature dependence to permeation by aqueous solutions—A study of lower consolute behavior," J. Polym. Sci. **13**, 2551–2570 (1975).
[41]Y. Guo, H. S. Patanwala, B. Bognet, and A. W. Ma, "Inkjet and inkjet-based 3D printing: Connecting fluid properties and printing performance," Rapid Prototyp. J. **23**, 562–576 (2017).
[42]P. Yang, W. bin Shen, E. Albert Reece, X. Chen, and P. Yang, "High glucose suppresses embryonic stem cell differentiation into neural lineage cells," Biochem. Biophys. Res. Commun. **472**, 306–312 (2016).
[43]M. E. Mor, A. Harvey, M. Familari, M. St Clair-Glover, S. Viventi, R. U. de Iongh, F. J. Cameron, and M. Dottori, "Neural differentiation medium for human pluripotent stem cells to model physiological glucose levels in human brain," Brain. Res. Bull. **173**, 141–149 (2021).
[44]C. D. Sorrell and M. J. Serpe, "Reflection order selectivity of color-tunable poly(*N*-isopropylacrylamide) microgel based etalons," Adv. Mater. **23**, 4088–4092 (2011).
[45]G. Kontaxi, T. Lugtmeijer, M. Serpe and H. Bazyar (2025). "Data underlying the paper: Inkjet-printed microgel-based etalon sensor," 4TU. https://doi.org/10.4121/0d5f9f9a-a71e-4e30-9144-f239d48a9543